Advanced tailings dam performance monitoring with seismic noise and stress models

Susanne Ouellet (susanne.ouellet2@ucalgary.ca)
University of Calgary https://orcid.org/0000-0001-8240-2916
Jan Dettmer
Uni Calgary https://orcid.org/0000-0001-8906-8156
Gerrit Olivier
University of Tasmania
Tjaart de Wit
Institute of Mine Seismology
Matthew Lato
BGC Engineering Inc.

Article

Keywords:

Posted Date: June 7th, 2022

DOI: https://doi.org/10.21203/rs.3.rs-1647118/v1

Abstract

Tailings dams retain the waste by-products of mining operations and are amongst the world's largest engineered structures. Recent tailings dam failures highlight important gaps in current monitoring methods and a pressing need to advance research on tailings dam monitoring technologies, considering growth predictions for the mining of metals. At an active tailings dam in northern Canada, we combine ambient noise interferometry with a quantitative stress model to monitor shear wave velocity (V_s) changes. Changes in seismic velocities of less than 1% correlate strongly with water level fluctuations at the adjacent tailings pond. A stress model, calibrated using pond level recordings and V_s profiles obtained from cone penetration tests, demonstrates that the seismic velocity changes obtained with ambient noise interferometry are predominantly changes in V_s. Furthermore, this model constrains V_s changes to a depth of ~16 m, corresponding to uncompacted tailings below the dam. As V_s is used to assess the liquefaction potential of soils, this method provides important advances for understanding changes in dam performance over time.

Introduction

Global demand for minerals is rising, with additional pressure on supply driven by the transition to renewable energy sources[1,2]. Alongside declining ore grades, this demand is increasing the volume of waste material, known as tailings, produced by the mining industry[1–3]. Tailings dams, designed to retain the waste by-products of mining, are among some of the largest engineered structures in the world[4]; there are an estimated 8,100 tailings facilities worldwide[3]. Tailings dams are designed and constructed under similar regulations as conventional water storage dams in many industrialized nations[4]. However, the likelihood of tailings dam failures is approximately two orders of magnitude higher, and the risk of future tailings dam failures is projected to increase[5,6]. The 2019 Brumadinho, Brazil tailings dam failure caused over 270 deaths, was an environmental disaster, and increased public scrutiny of tailings dams worldwide[3,7,8]. Forensic investigations of the failure classified it as a flow liquefaction event and indicated that the extensive monitoring instrumentation installed was inadequate to detect any significant changes prior to the failure[9]. This highlights the current challenges faced by geotechnical engineers to appropriately monitor these structures.

Ambient noise interferometry (ANI) is a geophysical technique that relies on the reconstruction of the impulse response of a wavefield by cross correlating the naturally occurring noise signals between a pair of seismic sensors, where one acts as a virtual source and the other as a receiver[10,11]. The wavefield includes coda waves in the later portion of the seismogram. Coda waves represent scattered waves that have spent more time propagating within the medium, and are more sensitive to seismic velocity changes[10,12]. By monitoring temporal changes in the coda portion of the wavefield propagating between the sensors, relative changes in seismic velocities are measured, commonly referred to as dv/v. This method has been used to monitor volcanoes, landslides, and dams[1–5].

Remote sensing methods, particularly satellite-based interferometric synthetic aperture radar, are increasingly being used to support tailings dam monitoring[6–10]. Alternatively, geophysical-based monitoring methods detect changes in the subsurface that aren't measurable using remote sensing methods[11–15]. Although geophysical-based methods also have limitations, they complement tailings dam monitoring when combined with remote sensing and downhole instrumentation (e.g. vibrating wire piezometers, slope inclinometers, etc.).

Shear wave velocities (V_s) are an important parameter for evaluating the liquefaction susceptibility of tailings materials[16,17]. Industry standard methods for obtaining V_s for liquefaction assessments include in-situ measurements with seismic cone penetration testing (sCPT), geophysical methods such as spectral analysis of surface waves, downhole and crosshole tests, and laboratory measurements using bender elements or resonant column tests[18]. These methods are generally used to characterize site conditions at one point in space and time, as multiple acquisitions are costly and time-consuming. Furthermore, differences in methods can lead to conflicting results[19,20]. This makes ANI an attractive method for geotechnical applications, to improve understanding of how V_s may change over time.

We employ ANI using an array of twenty-five geophones at an active mine site in northern Canada over a two-month period during summer. Site stratigraphy from nearby boreholes with sCPT data is used to constrain an effective stress model and improve understanding of the depth sensitivity of the ANI method. Our results demonstrate that seismic ambient noise monitoring coupled with an effective stress model provides new information about dam performance by resolving small changes in $V_{s,}$ and inferring where these changes occur. These advances pave the way for monitoring temporal and spatial changes of the stability and liquefaction potential of tailings dams, which could profoundly improve how these structures are monitored in the future.

Results

Seismic velocity changes and environmental site data

The study site is located at an active mine site, and a tailings pond is located ~ 200 m North of the geophone array (Fig. 1). Pond levels fluctuated throughout the data acquisition period and are controlled both by environmental and operational factors. We acquired vertical-component waveform data from twenty-five 5Hz geophones in a T-shaped array during active and inactive construction periods, from June to early August 2020 (Fig. 1). As ANI requires coherent cross-correlation waveforms and the active construction period resulted in incoherencies, these were removed from the dataset and only inactive construction period seismic data (three hours recorded per day) were relied on for further processing (**Fig S1**).

Standard ANI processing methodologies were applied to obtain seismic velocity changes (dv/v) (see **Methods**). The dv/v estimates were compared with other site information, including: tailings pond levels,

daily rainfall, atmospheric pressures and temperature data. During the monitoring period, three main trends are observed: (1) a dv/v increase of ~ 0.6% over the first month of recording coincides with decreasing water levels at the pond; (2) a dv/v decrease > 0.5% in the five days following the highest daily rainfall during the monitoring period; and (3) a dv/v recovery to the pre-rainfall levels in the final week of data acquisition (Fig. 2).

Effective stress model

We modelled relative changes in V_s, (dV_s/V_s) to validate our dv/v estimates by implementing a known relationship between V_s and effective vertical stress for granular soils. This relationship can be expressed as a power law, and is dependent on the polarization and propagation direction of shear waves[21–23]. For effective vertical stress, V_s is represented as

$$V_s = \alpha \sigma'^{\beta}_{v} \quad (1)$$

where α and β represent material constants, and σ'_v is the effective vertical stress[24,25]. The material constant α represents the shear wave velocity at σ'_v equal to 1 kPa, and β is a measure of the stress-level dependency to shear waves, empirically given[24] as

$$\beta = 1.01 - 0.18 \times \ln\alpha \quad (2)$$

Here, β incorporates both interparticle contact behavior and fabric changes. It approaches 0 for a cemented soil, 0.25 for rough, angular particles or spherical particles with contact yield, and 0.75 for contacts governed by Coulombian forces[23]. We obtained site-specific α and β parameters for the various stratigraphic units by performing a power-law regression analyses with bootstrap sampling, using V_s and σ'_v data obtained from 52 sCPTs completed in 2017 and 2018 (Fig. 3; **Table S-1**). Power-law regression analyses, undertaken for the compacted tailings and glaciolacustrine clay unit, are shown in Figs. S-3 and S-4. Additional details of statistical analyses are described in **Methods**.

Estimates of daily effective vertical stresses were inferred from daily resampled pond data using Eq. (6). These estimates, alongside site-specific α and β parameters (**Table S-1)** were input into Eq. (1) to obtain daily V_s. Relative changes in daily V_s were obtained, treating depths *z* as an unknown and varying it from near surface to bedrock depths (~ 39 m), using

$$\frac{dV_s}{V_s} = \frac{V_s - \bar{V}_s}{\bar{V}_s}$$

3

,

where $\bar{V}_s$ is the mean of all daily V_s estimates obtained with Eq. (1). The L1 norm was computed fitting the dV_s/V_s prediction to the dv/v results. A grid search over *z* produced a minimum misfit for *z* equal to 15.7 m (**Fig S-5**). Bootstrap analyses followed by Monte Carlo sampling were used to estimate uncertainties of the depth z obtained, with 95% confidence intervals from 14.1 m to 17.4 m (see **Methods** for details). Figure 3 shows the predicted dV_s/V_s results from the effective-stress model for the optimal *z* and dv/v results from ANI. The close agreement illustrates that the model successfully explains the ANI results to be predominantly changes in V_s, and that changes are occurring in the topmost 16 m of the structure. This primary sensitivity to shear waves is in agreement with the theoretical results for a Poisson medium[26]. Importantly, dominant sensitivity to V_s permits ANI results to be interpreted in terms of dam performance.

Discussion

Our dv/v estimates suggest that effective stress changes, attributed to changes in pond levels, have the strongest influence on dv/v, as no meaningful correlations are observed between dv/v and borehole temperature or barometric pressure data. This is consistent with other results[27,28]. Using a two-dimensional thermoelastic strain model, Tsai[27] demonstrated that hydrologic variations likely dominate dv/v estimates over thermoelastic effects. Furthermore, Clements and Denolle[28] modelled seasonal thermoelastic strains for dv/v monitoring and found that these strains had a much lower effect on the wavespeed perturbation than hydrological effects. Fokker et al.[29] present a physics-based model to show that changes in shear wave velocities are primarily caused by fluctuations in effective stress through changes in the shear modulus. Their approach relies on modelling changes in seismic surface wave velocity using a spectral element method[30]. In comparison, our model is based on empirical equations (Eq. (7)) from fundamental principles of soil mechanics, effective for near surface applications in granular soils. The application of empirical relationships is attractive for tailings dams, since site-specific sCPT data are typically available.

Our effective stress model is able to replicate the three main trends visible in the dv/v curve (Fig. 2); however, some discrepancies remain. Higher variability in individual dv/v traces is visible from July 15 to 17, 2020. We attribute this variability to nearby construction at the south of the geophone array, resulting in lower waveform coherencies over this period. Furthermore, due to a lack of groundwater level measurements near the geophone array, groundwater levels were inferred using data from the nearby

tailings pond. This may also contribute to discrepancies between dV_s/V_s predictions and the dv/v curve. Material heterogeneities (e.g. dam fill and tailings) along the seismic wave propagation paths are likely to further increase this discrepancy (Fig. 4).

We attribute the lack of meaningful correlations between dv/v estimates and temperature to the shorter (~ 41 day) data acquisition period. Over this period, the daily mean surface temperature fluctuated between 16˚C and 26˚C, with a mean temperature of 21˚C. Had our data acquisition continued during winter with more extreme temperature changes, these effects may have been visible in dv/v, as observed by others[31]. We chose to neglect the effects of barometric pressure within our effective stress model, considering the non-linearity of barometric pressures at depth (e.g. damping and time delay effects), dependent on soil properties and groundwater levels[32]. We also neglected the effects of suction in the unsaturated zone; assuming the soil behaves either fully saturated below the inferred ground water level or fully unsaturated, above the inferred ground water level. Further research and model development may improve understanding of the sensitivity of dv/v measurements to suction in the partially saturated zone.

The depth sensitivity of the dv/v estimates is dependent on the frequency band applied to the cross-correlations (5 to 15 Hz in this work). In an isotropic and homogeneous medium, most of the Rayleigh-wave energy at a frequency f is contained from surface to a depth z at approximately one third of a wavelength λ[33]. The average V_s in the dam fill (compacted tailings) and underlying tailings can be approximated as 300 m/s and 200 m/s, respectively, based on nearby sCPTs. As such, we estimate an average V_s of ~ 220 m/s over the topmost 39 m (i.e., from surface to bedrock) near our geophone array. Assuming a homogeneous medium, wavelengths for this V_s are between 15 m and 44 m, which suggest depth sensitivity between 5 m and 15 m. Our model estimates a depth sensitivity over the top ~ 16 m, accounting for the inhomogeneity of the structure, with a higher-velocity dam fill layer overlying lower-velocity tailings.

The α and β parameters obtained for the compacted tailings, coarse tailings and clay units were observed to have significantly higher uncertainties than for the fine tailings unit (**Fig S-5**). This is attributed to an overall lower number of samples and the heterogeneity of these layers. Heterogeneity, such as increased cobbles or gravel, as well as higher resistance, due to compaction of the compacted tailings, prevents advancement of the sCPT. This lowers the reliability of the sCPT measurements obtained through these layers.

Active mine sites are prime locations to study emerging monitoring methods such as ANI, as complementary site information (e.g. sCPTs, historical boreholes, weather station data), can be used to compare and validate results. At this site, data from 52 downhole sCPT measurements was used to parametrize an effective stress model to compare with dv/v estimates. As sCPTs are routinely carried out at many mine sites to assess the liquefaction potential of tailings, incorporation of sCPT data for model constraint allows for site-specific adaptation by mining practitioners. At sites without access to similar datasets, alternative geophysical techniques (e.g. multichannel analysis of surface waves) could be used to estimate site-specific constraints (α, β) to parametrize an effective stress model. Based on the general

agreement between the dv/v measurements and the dV_s/V_s model, our results demonstrate how ANI can be applied at a tailings dam site to provide highly sensitive (< 1%) measurements of in-situ changes of V_s alongside an approximation of depth sensitivity, without requiring advanced geomechanical models. By comparing the changes in V_s obtained from the model to the dv/v estimates, deviations between the modelled dV_s/V_s and the dv/v could be used to indicate potential anomalies (e.g. internal erosion) that aren't attributable to changes in groundwater levels. This approach could be used to alert to potential areas of concern, indicating where additional inspection and monitoring may be warranted. Furthermore, as V_s measurements are used in the evaluation of the liquefaction resistance of a soil[16], combining modelled dV_s/V_s with ANI could inform on changes in liquefaction potential of the in-situ tailings material and underlying foundation. For instance, as liquefaction involves a phase-change in the medium from a solid to liquid state, it follows that the shear wave velocity will also decrease dramatically[34]. Further research of liquefaction-type failures is needed to improve understanding of whether adequate warning time could be provided by monitoring changes in V_s[35].

The data processing steps described do not require high computing power, and could be used to efficiently process incoming data for ongoing monitoring purposes. For example, in an operational setting, geophone data could be processed using a three-day rolling average to reduce errors and limit uncertainties[14]. Combining information on changes in V_s with other monitored geotechnical parameters (e.g. pore pressures, deformation, seepage) could be used to advance overall tailings dam monitoring performance.

This methodology can be expanded towards monitoring greater extents (e.g. many kilometers) along linear infrastructure by combining ANI with distributed acoustic sensing (DAS) fiber optic technologies. At this mine site, existing telecoms optical fiber has been installed in the dam crest and research on the DAS dataset is underway using the methodology presented. The results of this research may have significant implications beyond monitoring tailings dams for other near-surface applications, such as permafrost engineering and landslide investigations. Even though some open questions remain, the advances presented in this manuscript show the potential to use ANI as a quantitative real-time tool and increase our understanding of the temporal evolution of the internal state of tailings dams.

Methods

Seismic recordings and cross-correlations

Nineteen geophones were installed in a northwest-southeast orientation along the tailings dam crest and six were installed in a northeast to southwest orientation extending into the tailings beach. Geophones were buried five to ten centimeters below ground to reduce the near surface effects of atmospheric pressure and temperature fluctuations. Geophones recorded for a 12-hour period per day. Nine hours of data were collected during active construction at the site, and three hours of data were collected when construction was not active.

The ambient noise recorded during active construction was highly directive and sources moved in time and space, resulting in incoherent cross-correlation waveforms. Therefore, cross-correlations are only considered from recording times without construction, three hours per day (00:00 to 03:00 UTC; Fig S-3). Sesimic data pre-processing included detrending, tapering, filtering and normalization[36]. Further details are in the **Supplementary information**. Each station pair combination (representing a virtual source and receiver) was cross-correlated using 20-second time windows. These windows were stacked over the three-hour inactive construction period to obtain daily cross-correlation waveforms. A reference cross-correlation waveform, required for computing dv/v, is the mean of all daily cross-correlations acquired over the data acquisition period (35 to 41 days depending on the battery life of the geophone). The dv/v measurement is plotted as a daily measurement at 01:30 UTC, to compare with the environmental site data recordings. The stretching methodology was applied to causal and acausal coda windows (+/- 0.5 seconds to +/- 3.5 seconds) to obtain dv/v measurements, and causal and acausal windows were averaged to improve signal to noise ratio[1, 37–39].

Effective stess model

Shear wave velocities (V_s) were obtained approximately every meter along sCPT profile by laterally striking a beam held in place by a normal load, using a sledgehammer. Average V_s are ~ 300 m/s in the compacted tailings material and ~ 200 m/s in the tailings and underlying material, up until refusal. A generalized stratigraphy model based on historical borehole data is shown in **Fig. 4a**.

The velocity of shear waves traveling within a soil depends on the effective confining stress, saturation, and mass density[23]. For a homogeneous and isotropic medium, V_s can be expressed as a function of the small strain shear modulus (G_{max}) and the bulk density of the soil (ρ),

$$V_s = \sqrt{\frac{G_{max}}{\rho}}$$

4

The principle of effective stress[40] defines the stress experienced by the soil skeleton that controls deformation. In a one-dimensional model, the effective vertical confining stress is equal to the overburden stress minus the pore pressure

$$\sigma_V^{'} = \sigma_V - u$$

5

,

where σ_V is the total vertical stress and the pore pressure u is obtained from

$$u = \gamma_w\left(z - d_w\right),$$

6

where γ_w is the unit weight of water (9.81 kN/m^3) and d_w is the depth to the inferred groundwater level, relative to the dam crest elevation. In Eq. (5), σ_v can be approximated as the sum of the unit weights of each layer, multiplied by the thickness of that layer. Using the resampled daily pond data, we estimate σ'_v at depths varying from surface to the approximate bedrock depth at 39 m, for each day. Equations to obtain the total vertical stress σ_v for z in each layer, relative to the dam crest, are

$$\sigma_v(z) = \begin{cases} \gamma_{df} z, z < d_w \\ \gamma_{df}\left(d_w\right) + \gamma_{df,sat}\left(h_1 - d_w\right), d_w < z < h_1 \\ \gamma_{df}\left(d_w\right) + \gamma_{df,sat}\left(h_1 - d_w\right) + \gamma_{t,sat}\left(z - h_1\right), h_1 < z < h_2 \\ \gamma_{df}\left(d_w\right) + \gamma_{df,sat}\left(h_1 - d_w\right) + \gamma_{t,sat}\left(h_2\right) + \gamma_{GLU,sat}\left(z - h_2\right), z > h_2 \end{cases}$$

7

,

where d_w is the depth to the inferred groundwater level, h_1 is the distance from surface to the dam fill and tailings boundary, and h_2 is the distance from surface to the tailings and clay boundary (Fig. 3). Unit weights are shown as γ_{df} and $\gamma_{df,sat}$, representing the moist and saturated dam fill, $\gamma_{t,sat}$, representing the underlying tailings, and $\gamma_{GLU,sat}$ representing the underlying glaciolacustrine clay unit.

Bootstrap analyses were performed on α and β parameters obtained from the power regression analyses. A total of 150,000 bootstrap simulations were performed to obtain probability distributions for α, β parameters of each unit (Fig. 4). Monte Carlo simulations were then performed (50,000 iterations) to randomly select from the empirical cumulative distribution function of the α, β parameters obtained from bootstrap sampling. A depth z, representing the minimum L1 misfit between dv/v estimates and the dV_s/V_s model, was obtained for each simulation. The resulting probability distribution of depth z is shown in **Fig S-6**.

Declarations

Acknowledgments, Samples, and Data

The authors gratefully acknowledge the support of industry partners on this research, made possible under a Mitacs Accelerate grant. BGC Engineering acted as the industry sponsor of this research project and provided technical review and support. The mining client granted site access to install the geophones

and provided field support. The Institute of Mine Seismology provided the geophones, in addition to technical review and support.

Open-source codes were used and modified to compute the cross-correlations and produce several of the figures in this report. This includes the stretching algorithm used to obtain dv/v time-series data[41], and the ROSES2021 code for **Fig. S-3a** and **S-3b**, courtesy of Jelle Assink[42]. Several of the available codes used for this work are available on the primary author's Github page at github.com/smouellet/ani-monitoring.

Author contributions

SO led study design, carried out field work, analyzed data, wrote the manuscript text, and prepared all figures. JD provided supervision, review and editing of the manuscript. GO, TdW and ML provided feedback on the study, and reviewed and edited the manuscript.

References

1. Sens-Schönfelder, C. & Wegler, U. Passive image interferemetry and seasonal variations of seismic velocities at Merapi Volcano, Indonesia. Geophysical Research Letters **33**, (2006).
2. Planès, T., Larose, E., Rossetto, V. & Margerin, L. Imaging multiple local changes in heterogeneous media with diffuse waves. J Acoust Soc Am **137**, 660–667 (2015).
3. Mainsant, G. *et al.* Ambient seismic noise monitoring of a clay landslide: Toward failure prediction. Journal of Geophysical Research: Earth Surface **117**, (2012).
4. Bièvre, G. *et al.* Influence of environmental parameters on the seismic velocity changes in a clayey mudflow (Pont-Bourquin Landslide, Switzerland). Engineering Geology **245**, 248–257 (2018).
5. Olivier, G., Brenguier, F., de Wit, T. & Lynch, R. Monitoring the stability of tailings dam walls with ambient seismic noise. Leading Edge **36**, 350a1-350a6 (2017).
6. Grebby, S. *et al.* Advanced analysis of satellite data reveals ground deformation precursors to the Brumadinho Tailings Dam collapse. Communications Earth & Environment **2**, (2021).
7. Lumbroso, D., Davison, M., Body, R. & Petkovšek, G. Modelling the Brumadinho tailings dam failure, the subsequent loss of life and how it could have been reduced. Natural Hazards and Earth System Sciences **21**, 21–37 (2021).
8. Lumbroso, D. *et al.* The potential to reduce the risks posed by tailings dams using satellite-based information. International Journal of Disaster Risk Reduction **38**, (2019).
9. Silva Rotta, L. H. *et al.* The 2019 Brumadinho tailings dam collapse: Possible cause and impacts of the worst human and environmental disaster in Brazil. International Journal of Applied Earth Observation and Geoinformation **90**, (2020).
10. Carlà, T. *et al.* Perspectives on the prediction of catastrophic slope failures from satellite InSAR. Scientific Reports **9**, (2019).

11. Whiteley, J. S., Chambers, J. E., Uhlemann, S., Wilkinson, P. B. & Kendall, J. M. Geophysical Monitoring of Moisture-Induced Landslides: A Review. Reviews of Geophysics vol. 57 106–145 (2019).
12. Fan, X. *et al.* Recent technological and methodological advances for the investigation of landslide dams. Earth-Science Reviews vol. 218 (2021).
13. Michalis, P. & Sentenac, P. Subsurface condition assessment of critical dam infrastructure with non-invasive geophysical sensing. Environmental Earth Sciences **80**, (2021).
14. le Breton, M., Bontemps, N., Guillemot, A., Baillet, L. & Larose, É. Landslide monitoring using seismic ambient noise correlation: challenges and applications. Earth-Science Reviews vol. 216 (2021).
15. Hamlyn, J. E. & Bird, C. L. Geophysical investigation and monitoring of dam infrastructure. Dams and Reservoirs **31**, 57–66 (2021).
16. Andrus, R. D. & Stokoe, K. H. Liquefaction Resistance of Soils from Shear-wave Velocity. Journal of Geotechnical and Geoenvironmental Engineering **126**, 1015–1023 (2000).
17. Youd, T. L. *et al.* Liquefaction Resistance of Soils: Summary Report from the 1996 NCEER/NSF Workshops on Evaluation of Liquefaction Resistance of Soils. Journal of Geotechnical and Geoenvironmental Engineering **127**, 817–833 (2001).
18. Hussien, M. N. & Karray, M. Shear wave velocity as a geotechnical parameter: An overview. Canadian Geotechnical Journal **53**, 252–272 (2016).
19. Butcher, A. P. & Powell, J. J. M. Determining the modulus of the ground from in-situ geophysical testing. in *Proc., 14th Int. Conf. on Soil Mechanics and Foundation Engineering* 449–452 (1997).
20. Ulrich, B. F. & Coffin, J. G. Characterization of Unsaturated Tailings and its Effects on Liquefaction. in *Proceedings of Tailings and Mine Waste* (2017).
21. Hardin, B. O. & Drnevich, V. P. Shear modulus and damping in soils: Measurement and Parameter Effects. Journal of the Soil Mechanics and Foundations Division **8977**, 603–624 (1972).
22. Cascante, G. & Santamarina, J. C. Interparticle Contact Behavior and Wave Propagation. Journal of Geotechnical Engineering **122**, 831–839 (1996).
23. Santamarina, J. C., Klein, K. A. & Fam, M. A. *Soils and Waves: Particulate Materials Behavior, Characterization and Process Monitoring*. (Wiley, 2001).
24. Ku, T., Subramanian, S., Moon, S.-W. & Jung, J. Stress Dependency of Shear-Wave Velocity Measurements in Soils. J. Geotech. Geoenviron. Eng. **143**, (2017).
25. Cha, M. *et al.* Small-Strain Stiffness, Shear-Wave Velocity, and Soil Compressibility. (2014) doi:10.1061/(ASCE)GT.1943.
26. Snieder, R. Coda wave interferometry and the equilibration of energy in elastic media. Physical Review E - Statistical Physics, Plasmas, Fluids, and Related Interdisciplinary Topics **66**, 8 (2002).
27. Tsai, V. C. A model for seasonal changes in GPS positions and seismic wave speeds due to thermoelastic and hydrologic variations. Journal of Geophysical Research: Solid Earth **116**, (2011).
28. Clements, T. & Denolle, M. A. Tracking Groundwater Levels Using the Ambient Seismic Field. Geophysical Research Letters **45**, 6459–6465 (2018).

29. Fokker, E., Ruigrok, E., Hawkins, R. & Trampert, J. Physics-based relationship for pore pressure and vertical stress monitoring using seismic velocity variations. Remote Sensing **13**, (2021).
30. Hawkins, R. A spectral element method for surface wave dispersion and adjoints. Geophysical Journal International **215**, 267–302 (2018).
31. Steinmann, R., Hadziioannou, C. & Larose, E. Effect of centimetric freezing of the near subsurface on Rayleigh and Love wave velocity in ambient seismic noise correlations. Geophysical Journal International **224**, 626–636 (2021).
32. Schulz, W. H., Kean, J. W. & Wang, G. Landslide movement in southwest Colorado triggered by atmospheric tides. Nature Geoscience (2009) doi:10.1038/NGEO659.
33. Matthews, M. C., Hope, V. S. & Clayton, C. R. I. The use of surface waves in the determination of ground stiffness profiles. in *Proc. Instn. Civ. Engrs. Geotech. Eng.* 84–95 (1996).
34. Snieder, R. & van den Beukel, A. The liquefaction cycle and the role of drainage in liquefaction. Granular Matter **6**, 1–9 (2004).
35. Yang, J., Liang, L. B. & Chen, Y. Instability and liquefaction flow slide of granular soils: the role of initial shear stress. Acta Geotechnica **17**, 65–79 (2022).
36. Bensen, G. D. *et al.* Processing seismic ambient noise data to obtain reliable broad-band surface wave dispersion measurements. Geophysical Journal International **169**, 1239–1260 (2007).
37. Lobkis, O. I. & Weaver, R. L. Coda-Wave Interferometry in Finite Solids: Recovery of P-to-S Conversion Rates in an Elastodynamic Billiard. Physical Review Letters **90**, 4 (2003).
38. Hadziioannou, C., Larose, E., Coutant, O., Roux, P. & Campillo, M. Stability of Monitoring Weak Changes in Multiply Scattering Media with Ambient Noise Correlation: Laboratory Experiments. (2009) doi:10.1121/1.3125345.
39. Obermann, A. & Hillers, G. Seismic time-lapse interferometry across scales. in *Advances in Geophysics* vol. 60 65–143 (Academic Press Inc., 2019).
40. Terzaghi, K. Die Berechnung der Durchlassigkeitsziffer des Tones aus Dem Verlauf der Hidrodynamichen Span-Nungserscheinungen Akademie der Wissenschaften in Wien. Mathematish-Naturwissen-SchaftilicheKlasse 125–138 (1923).
41. Viens, L., Denolle, M. A., Hirata, N. & Nakagawa, S. Complex Near-Surface Rheology Inferred From the Response of Greater Tokyo to Strong Ground Motions. Journal of Geophysical Research: Solid Earth **123**, 5710–5729 (2018).
42. Dannemann Dugick, F., Toney, L. & Goerzen, C. fdannemanndugick/roses2021: Citable (Version v0). Zenodo. (2021).

Figures

Figure 1

Site overview. **(a)** Geophone array overlain on lidar data (1 m contours, collected in November 2020). Location of subset of sCPTs used in regression analyses. Additional sCPTs used in analyses are not shown as they are outside of the figure extents. **(b)** Twenty-five geophone array (20 on dam crest, five on tailings beach), showing cross-section A-A'. **(c)** Cross-section A-A' of the tailings dam. The dashed black line shows approximation of dam fill and tailings extent for an upstream tailings facility, and does not represent actual delineated extents of fill and tailings.

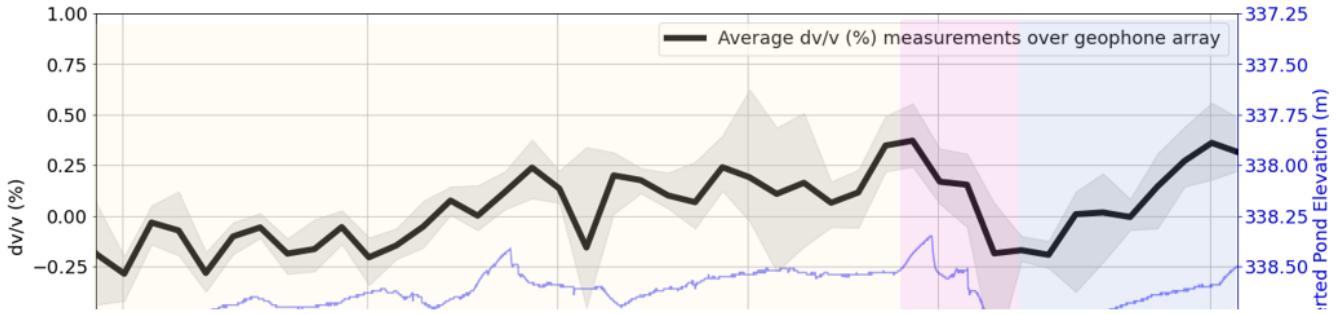

Figure 2

Seismic velocity changes (dv/v) plotted with pond levels, rainfall and barometric pressure. The upper graph shows average dv/v over the geophone array as a thick black line, with minimum and maximum extents of individual virtual sources averaged over all receiver combinations shaded in light grey. The nearby pond elevation is plotted on the same graph with an inverted y-axis, to illustrate the inverse correlation of the pond levels with dv/v. The lower graph shows the daily rainfall, barometric pressure and pond elevations. Three main trends are observed: (1) an increase in dv/v of up to ~0.6% over the first month of data acquisition coincides with a decrease in water levels at the nearby pond; (2) a decrease in

dv/v of over ~0.5% in the five-days following the highest daily rainfall observed over the monitoring period; and (3) a recovery in dv/v to the pre-rainfall levels in the final week of data acquisition.

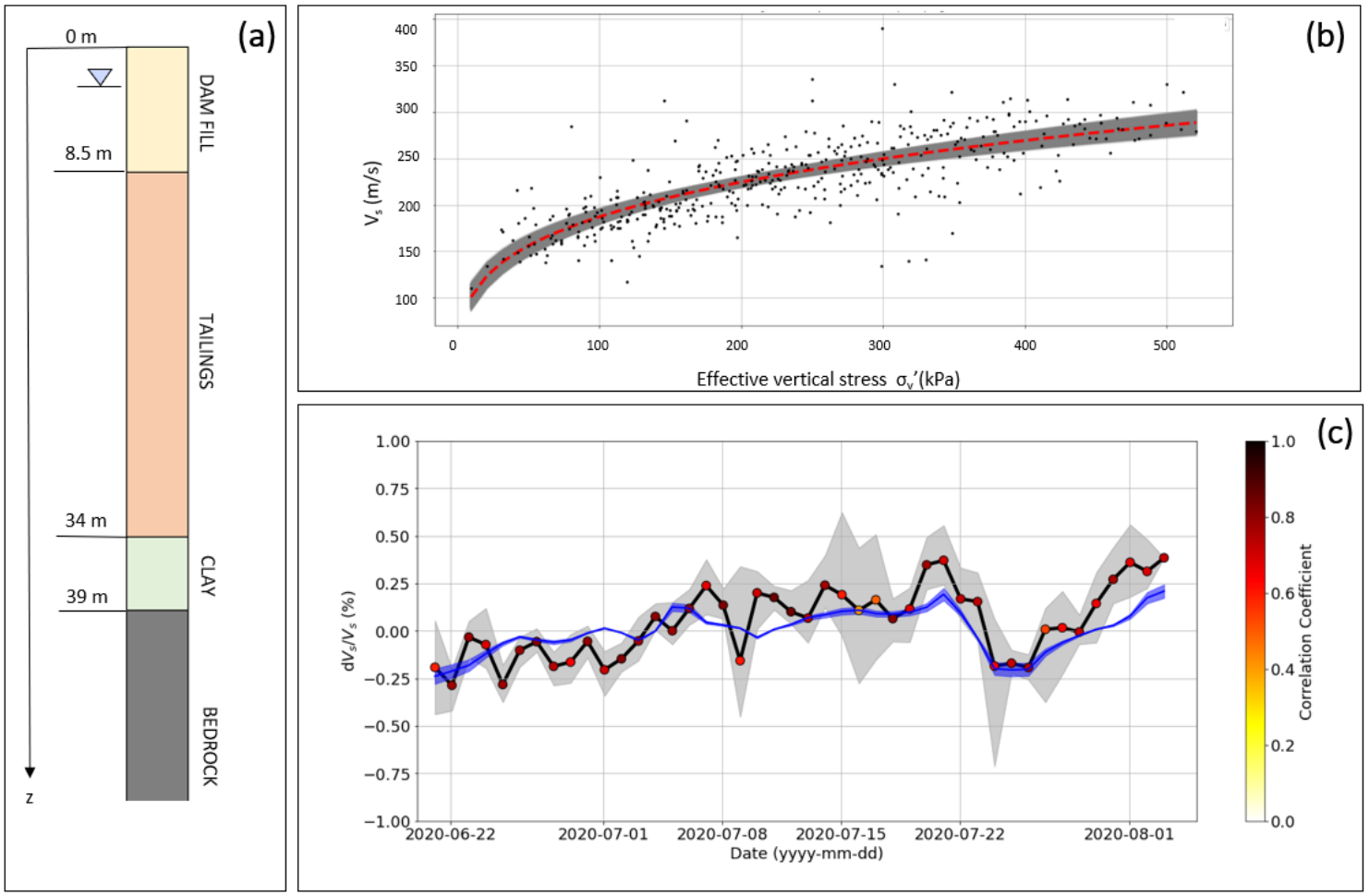

Figure 3

Main result. **(a)** Site stratigraphy obtained from historical borehole information. **(b)** Estimation of site specific and from power-law regression using V_s estimates from sCPT surveys and effective vertical stress for tailings material. Bootstrap analyses, shown in shaded grey, were used to obtain 95% confidence intervals of the

 and parameters. Regression results for compacted/coarse tailings and clay units are presented in Supplementary **Fig S3. (c)** Modelled dV_s/V_s based on

 and obtained from power-law regression for an optimized depth z in blue. Shaded blue area represents the maximum and minimum extents of 50,000 Monte Carlo simulations, and the blue line is the mean of all simulations. Average dv/v estimates over geophone array are shown as a black line, with gray shading representing maximum and minimum extents of individual virtual sources averaged over all receiver

combinations. The average correlation coefficient, plotted as a marker, shown between the reference correlation waveform and the stretched waveform.

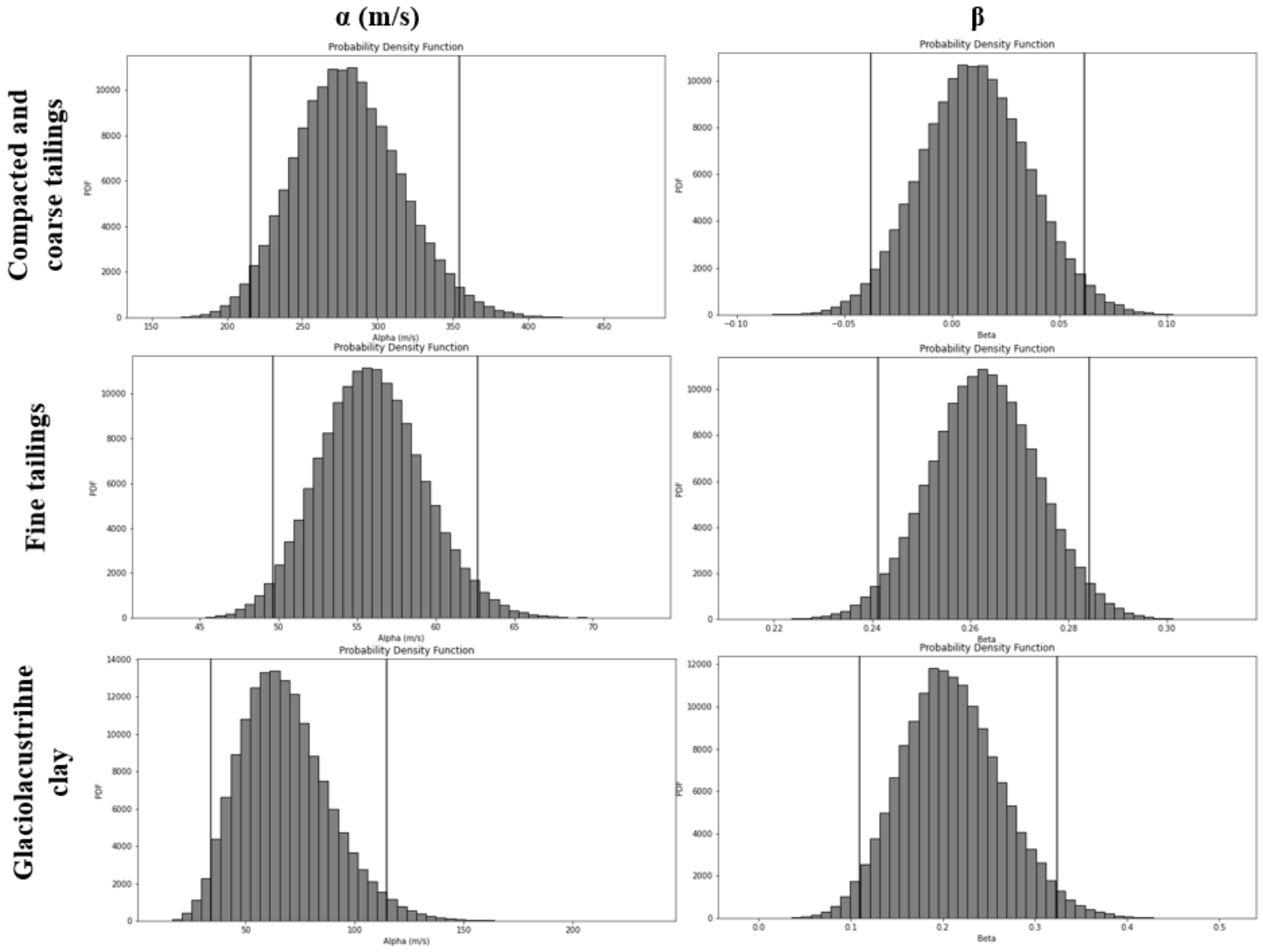

Figure 4

Probability density functions of α and β parameters showing 95% confidence intervals (black vertical lines) obtained from bootstrap sampling (150,000 samples).

Supplementary Files

This is a list of supplementary files associated with this preprint. Click to download.

- ANITailingsSuppl.docx